Int. J. Electrochem. Sci., 17 **(2022)** Article Number: 220745, doi: 10.20964/2022.07.44

International Journal of
ELECTROCHEMICAL
SCIENCE
www.electrochemsci.org

Multi–walled Carbon Nanotubes Modified Stainless Steel Fiber Felt Supported on Cobalt Electrode for N_2H_4 Electrooxidation in Alkaline Solution

Ran Liu[1,*], *Xinyue Zhao*[1], *Shuang Zhang*[1], *Hui Chen*[1], *Jinling Yin*[2]

[1] Department of Chemistry, School of Food Engineering, Harbin University, Harbin, 150086, P.R.China
[2] Key Laboratory of Superlight Materials and Surface Technology of Ministry of Education, College of Materials Science and Chemical Engineering, Harbin Engineering University, Harbin, 150001, P.R.China
[*]E-mail: liuran7907@163.com

Received: 3 April 2022 / *Accepted:* 6 May 2022 / *Published:* 6 June 2022

A multi-walled carbon nanotubes (MWCNTs) modified stainless steel fiber felt (SSFF) supported on cobalt (Co/MWCNTs@SSFF) electrode is synthesized through a simple synthetic strategy that involves a binder-free dipping/drying step to form a MWCNTs@SSFF substrate and a subsequent potentiostatic electrodeposition of Co. The N_2H_4 electrooxidation reaction on the Co/MWCNTs@SSFF electrode occurs through direct and indirect electrooxidation pathways. The Co/MWCNTs@SSFF electrode achieves a N_2H_4 electrooxidation peak current density of 97.1 mA cm^{-2} in 1 M KOH with 0.1 M N_2H_4, and this current density is far greater than that of a Co/SSFF electrode (29.7 mA cm^{-2}). In comparison with the Co/SSFF electrode, the Co/MWCNTs@SSFF electrode has a larger electrochemical active surface area (ECSA) as well as a lower activation energy (E_a) for N_2H_4 electrooxidation. The Co/MWCNTs@SSFF electrode exhibits good electrocatalytic properties due to the macroporous structure of the SSFF substrate, porous structure of the Co nanospheres and enhanced ECSA resulting from the MWCNTs modification.

Keywords: Cobalt; Stainless steel fiber felt; Multi–walled carbon nanotubes; N_2H_4 electrooxidation

1. INTRODUCTION

Environmental deterioration caused by the use of fossil fuels has become a major problem that humanity must face. Looking for an efficient and clean energy conversion technology has become a worldwide concern. Based on this background, fuel cells, as a clean and efficient power generation technology, have been the focus of attention.

A direct hydrazine fuel cell (DHFC) adopting hydrazine (N_2H_4) as fuel has the following merits

[1-3]. (1) The DHFC exhibits a higher theoretical electromotive force of 1.56 V than that of a direct methanol fuel cell. (2) N_2H_4 electrooxidation in alkaline solution generates only N_2 and H_2O (Eq. (1)), resulting in zero emissions and meeting the requirements for environmental protection. (3) In the process of N_2H_4 electrooxidation, species that poison the catalyst are not generated. The remarkable advantages of DHFC indicate that it is a new type of fuel cell with potential applications. However, the N_2H_4 electrooxidation reaction at the anode is a kinetically slow process and must be performed at a higher overpotential, resulting in a lower voltage efficiency. Therefore, designing and synthesizing an electrocatalyst that can sharply reduce the overpotential of the N_2H_4 electrooxidation reaction is the key to promoting the performance of DHFC.

$$N_2H_4 + 4OH^- \rightarrow N_2 + 4H_2O + 4e^- \quad (1)$$

At present, precious metals [4-6] are perceived as excellent electrocatalysts for N_2H_4 electrooxidation. However, their high prices and limited reserves greatly hinder the DHFC commercialization process. In view of this, the development of highly effective nonprecious catalysts that are expected to replace precious metal catalysts has become a popular issue in recent research [7-21]. Asazawa et al. [22] reported that the performance of a DHFC with Co as the anode catalyst was superior to that with Pt as the anode catalyst. Moreover, Asazawa et al. [23] studied the electrocatalytic properties of diverse metal electrodes (Pt, Au, Ag, Co, Cu, Ni and Fe) for N_2H_4 electrooxidation in alkaline solution. The results showed that Co displayed better electrocatalytic properties than those of Pt in the low overpotential range. Therefore, Co is a promising electrocatalyst for N_2H_4 electrooxidation.

Carbon–supported Co catalysts are common electrocatalysts for the N_2H_4 electrooxidation reaction [7,17]. Although carbon–supported Co catalysts display high electrocatalytic activities, they still have some drawbacks, such as their low mechanical strength and lack of macropores. Moreover, organic binders need to be added when the powder carbon-supported Co catalyst is made into an electrode by the conventional coating method. The introduction of organic binders increases the resistance of the catalyst, blocks the pores of the catalyst, and prevents the catalyst from fully contacting the collector or electrolyte, thus reducing the utilization of the catalyst. The N_2H_4 electrooxidation reaction occurs at the solid–liquid interface with gas generation. Considering the features of the N_2H_4 electrooxidation reaction, electrocatalysts for the N_2H_4 electrooxidation reaction should exhibit superior gas–liquid mass transfer performances. Therefore, electrocatalysts with porous structures are more suitable for catalyzing the N_2H_4 electrooxidation reaction. To solve the above challenges, a carbon material is coated on a conductive substrate with a porous structure to reduce not only the contact resistance between the carbon material and substrate but also the diffusion resistance. Among various conductive substrates, SSFF is widely used because of its high electroconductivity, macroporous structure and good ability to resist corrosion [24, 25].

Based on the above considerations, a distinctive SSFF modified with MWCNTs supported on Co electrode (Co/MWCNTs@SSFF) was synthesized. First, MWCNTs were coated on the surface of SSFF using a binder-free dipping/drying method. Then, Co species were directly electrodeposited onto MWCNTs/SSFF by a potentiostatic approach. To the best of our knowledge, research regarding the application of the Co/MWCNTs@SSFF electrode as an electrocatalyst for N_2H_4 electrooxidation in alkaline solution has not been reported. The as-synthesized Co/MWCNTs@SSFF electrode exhibited an excellent electrocatalytic capability for the N_2H_4 electrooxidation reaction. In addition, the kinetics

parameters of the N_2H_4 electrooxidation reaction on the Co/MWCNTs@SSFF sample were determined.

2. EXPERIMENTAL

2.1. Synthesis of the Co/MWCNTs@SSFF sample

A schematic diagram for synthesizing the Co/MWCNTs@SSFF sample is presented in Fig. 1. In the first step, a piece of SSFF (BZ15D, porosity of 78%, Xi'an Felt Metal Filter Material Co., Ltd.) with a geometric area of 1 cm^2 was impregnated into a 50 mL solution of 3 mg mL^{-1} MWCNTs (length of 5-15 μm, diameter of 20-40 nm, Shenzhen Nanotech Port Co., Ltd.) for 1 min. Then, the SSFF was removed from the MWCNTs suspension liquid and dried at 100 °C for 2 h. The impregnating-drying step was repeated four times until the surface of the SSFF substrate was coated with a thin layer of MWCNTs (denoted as MWCNTs@SSFF). The MWCNT loading was approximately 4 mg. Before preparing the MWCNTs@SSFF substrate, the SSFF was successively and ultrasonically washed in CH_3COCH_3 and C_2H_5OH, rinsed with deionized water and dried at 60°C for several hours. The MWCNTs must be cleaned by an acid. A total of 500 mg of MWCNTs was refluxed for 5 h at 60°C in a mixed solution containing 68% HNO_3 and 98% H_2SO_4 at a volumetric ratio of 1:3 with vigorous stirring. Then, the above solution was washed using distilled water until the solution reached a neutral pH. In the second step, Co particles were electrodeposited onto the MWCNTs@SSFF surface (denoted as Co/MWCNTs@SSFF) by electrochemical deposition with a constant controlled current of -2 mA for 3200 s in 0.005 M $CoSO_4$ and 0.1 M $(NH_4)_2SO_4$. This step was completed with a three-electrode setup that used MWCNTs@SSFF as the working electrode, a Pt plate and a saturated Ag/AgCl electrode as the counter and reference electrodes, respectively.

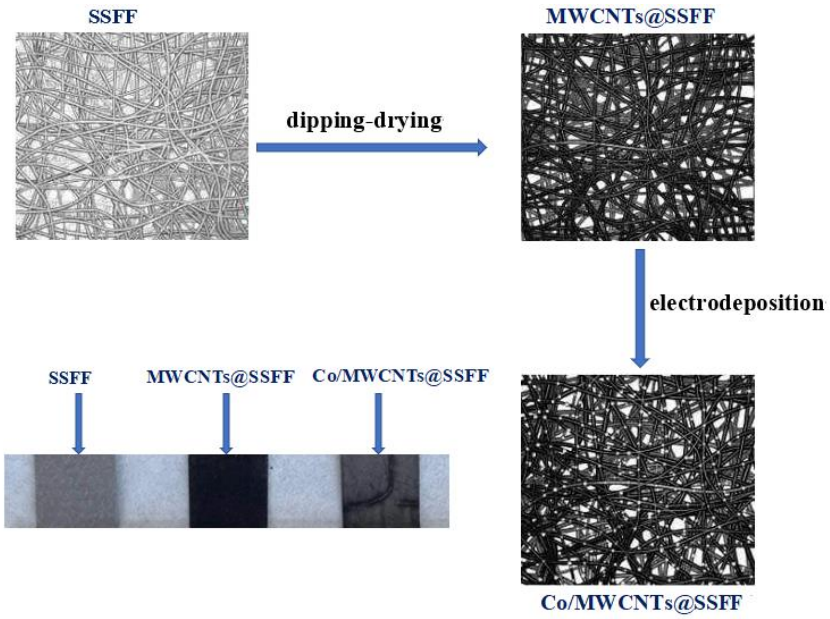

Figure 1. Schematic diagram for synthesizing the Co/MWCNTs@SSFF sample.

For comparison, Co particles were directly electrodeposited onto the SSFF substrate surface (denoted as Co/SSFF) by electrochemical deposition with a constant controlled current of -2 mA for 3200 s in 0.005 M $CoSO_4$ and 0.1 M $(NH_4)_2SO_4$.

2.2. Characterization

X-ray diffraction (XRD) data concerning the Co/MWCNTs@SSFF were gained from a Bruker D8 Advance diffractometer using a Cu Kα radiation source. The surface morphologies of the electrode materials were determined through a scanning electron microscope (SEM, HITACHI SU8010) equipped with an energy dispersive X-ray spectroscopy (EDS) addon and transmission electron microscopy (TEM, FEI, Tecnai G2 F20).

2.3. Electrochemical testing

Information concerning the electrocatalytic properties of the as-synthesized samples for N_2H_4 electrooxidation was collected using cyclic voltammetry (CV) and chronoamperometry (CA). Electrochemical testing was accomplished in a three-electrode setup that was controlled by a CHI 760E electrochemical analyzer (Shanghai Chenhua Instrument Co., Ltd). The as-synthesized samples were adopted as the working electrodes. A Pt plate and a saturated Ag/AgCl electrode were adopted as the counter and reference electrodes, respectively. Unless otherwise stated, the electrochemical tests were completed at 22±1°C. The current density was obtained by normalizing it to the geometric area of the as-synthesized sample.

3. RESULTS AND DISCUSSION

3.1. Characterization

The SEM images of the SSFF (a, b), MWCNTs@SSFF (c, d) and Co/MWCNTs@SSFF electrodes (e-g) together with the TEM image of the Co/MWCNTs@SSFF electrode (h) are given in Fig.2. As observed from Fig. 2a, the SSFF exhibits a three-dimensional network configuration, which can provide a short pathway for contact between the electrolyte and electrode. The surface of the SSFF substrate is rough (Fig. 2b), which is favorable for the MWCNT coating. As seen in the figure, a thin layer of MWCNTs is evenly coated on the SSFF fibers (Fig. 2c). The enlarged SEM image of MWCNTs@SSFF (Fig. 2d) clearly shows that the MWCNTs are connected together to form a porous network structure. Coating the MWCNTs on the SSFF substrate can significantly augment the surface area. Fig. 2e and 2f reveal that the Co catalyst is uniformly grown on the MWCNTs@SSFF surface and has a spherical structure with diameters ranging from 150-500 nm. The Co nanospheres consist of nanosheets and nanoparticles (Fig. 2g). As shown in Fig. 2h, a sheet structure accompanied by some wrinkles can be seen in Co/MWCNTs@SSFF.

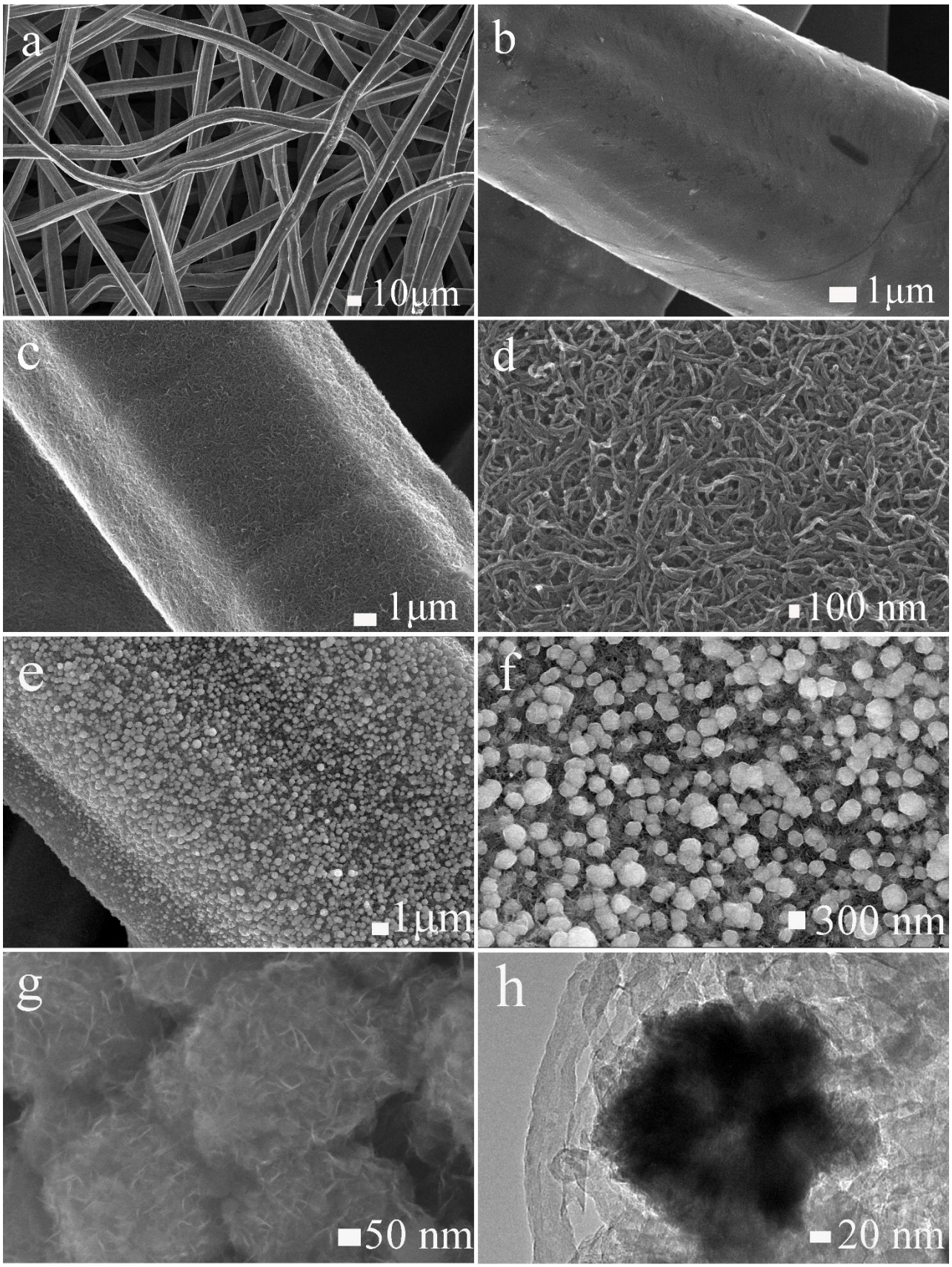

Figure 2. SEM images of the SSFF (a, b), MWCNTs@SSFF (c, d) and Co/MWCNTs@SSFF electrodes (e-g); TEM image of the Co/MWCNTs@SSFF electrode (h).

Fig. 3 gives the XRD image of the Co/MWCNTs@SSFF sample. The broad diffraction peak that appears at approximately 26° is attributed to the MWCNTs [26]. Three sharp diffraction peaks that appear at 43.6°, 50.8° and 74.7° are attributable to the (111), (200) and (220) planes of the austenitic steel (PDF No. 33-0945), respectively [27]. The four diffraction peaks at 41.68°, 44.5°, 47.5°, and 75.9° correspond to the (100), (002), (101), and (110) planes of Co (PDF No. 05-0727), respectively.

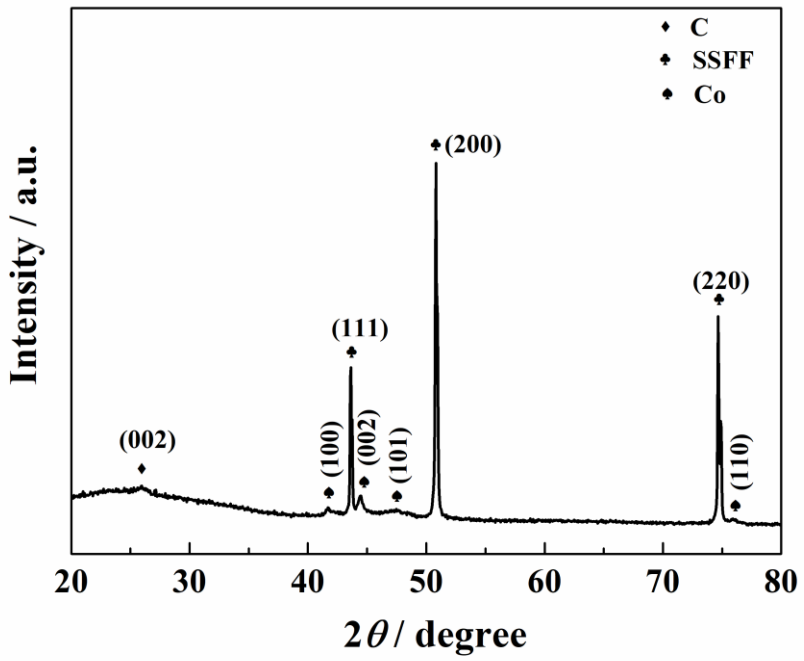

Figure 3. XRD image of the Co/MWCNTs@SSFF sample.

Fig. 4 presents the SEM image (a) and the EDS spectrogram (b) with the corresponding elemental distributions of Co (c) and C (d) of the Co/MWCNTs@SSFF sample. The characteristic peaks of C and Co observed in the EDS spectrogram further suggest the existence of the MWCNT coating layer and Co particles. The characteristic peaks of Fe, Cr, Ni and Mn are due to the SSFF substrate. Additionally, the O that appears in the spectrogram is derived from the functional groups formed on the MWCNT surface in the preprocessing procedure [28]. As seen from Fig. 4c, Co particles are deposited on the MWCNT surface. The distribution of C is dispersed (Fig. 4d), indicating that the MWCNTs are not completely covered by Co.

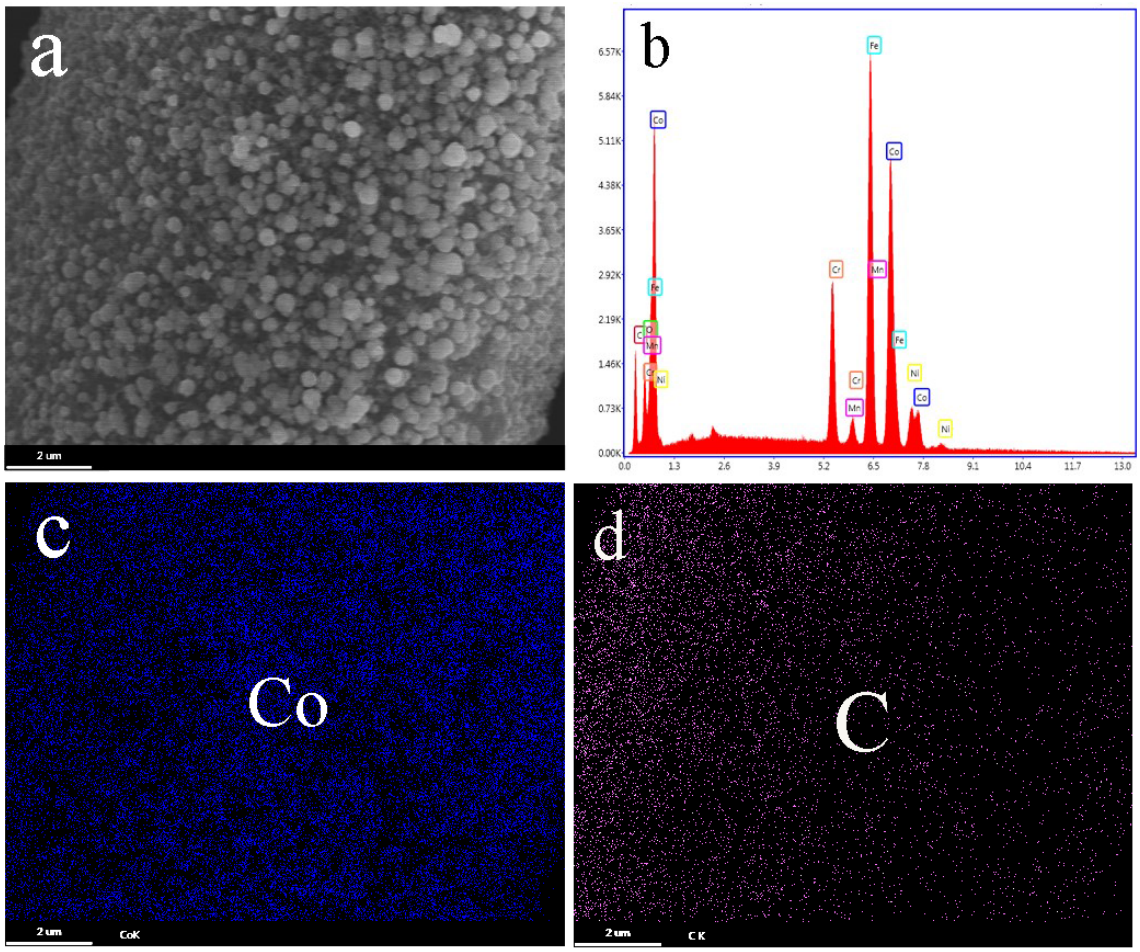

Figure 4. SEM image (a), EDS spectrogram (b) and corresponding elemental distributions of Co (c) and C (d) of the Co/MWCNTs@SSFF sample.

3.2. Electrochemical behavior of the Co/MWCNTs@SSFF electrode

The electrocatalytic activities of the SSFF, MWCNTs@SSFF and Co/MWCNTs@SSFF electrodes toward N_2H_4 electrooxidation were evaluated using cyclic voltammograms in 1 M KOH with 0.1 M N_2H_4 at 10 mV s^{-1}, as exhibited in Fig. 5. Clearly, no obvious oxidation/reduction currents were observed with the SSFF and MWCNTs@SSFF electrodes, suggesting that the SSFF and MWCNTs@SSFF electrodes have no notable electrocatalytic properties for N_2H_4 electrooxidation. As seen, there are two oxidation peaks in the cyclic voltammogram of the Co/MWCNTs@SSFF electrode. The N_2H_4 electrooxidation reaction on the as-synthesized Co/MWCNTs@SSFF electrode occurs through direct (Eq. (1)) and indirect electrooxidation ways (Eq. (2)-(3)). In the indirect way, H_2 generated from N_2H_4 decomposition (Eq. (2)) is electrochemically oxidized in an alkali solution to H_2O (Eq. (3)). The anodic peak (-0.74 V) can be attributable to the electrooxidation of H_2 generation from N_2H_4 decomposition. The anodic peak (-0.65 V) is ascribed to N_2H_4 electrooxidation. These results agree with our previous work [29]. Additionally, a reduction peak was not observed in the cyclic voltammogram, indicating the irreversibility of N_2H_4 electrooxidation on the Co/MWCNTs@SSFF electrode.

$$N_2H_4 \rightarrow N_2 + 2H_2 \qquad (2)$$

$$2H_2 + 4OH^- \rightarrow 4H_2O + 4e^- \quad (3)$$

For comparison, a Co/SSFF electrode was fabricated by the same method except that the MWCNT coating step was omitted. Clearly, the N_2H_4 electrooxidation reaction on the Co/SSFF electrode also follows direct and indirect pathways. The N_2H_4 electrooxidation peak current density of the Co/MWCNTs@SSFF electrode is 97.1 mA cm^{-2}, which far exceeds that of the Co/SSFF (29.7 mA cm^{-2}). These results demonstrate that the Co/MWCNTs@SSFF electrode has superior electrocatalytic properties. The electrocatalytic property of the Co/MWCNTs@SSFF electrode was compared with that of some cobalt-based catalysts and metal nanoparticles supported on MWCNTs catalysts reported in the literature for N_2H_4 electrooxidation (Table 1). It should be noted that the scan rate, N_2H_4 concentration and electrolyte concentration affect the electrocatalytic performance of the catalyst for N_2H_4 electrooxidation. Because various research teams adopted various experimental parameters to assess the electrocatalytic activities of the catalysts reported in their works, an exact comparison was impossible. As seen from Table 1, the Co/MWCNTs@SSFF electrode exhibited a better electrocatalytic performance for N_2H_4 electrooxidation than that of many cobalt-based catalysts and metal nanoparticles supported on MWCNTs catalysts reported in the literature.

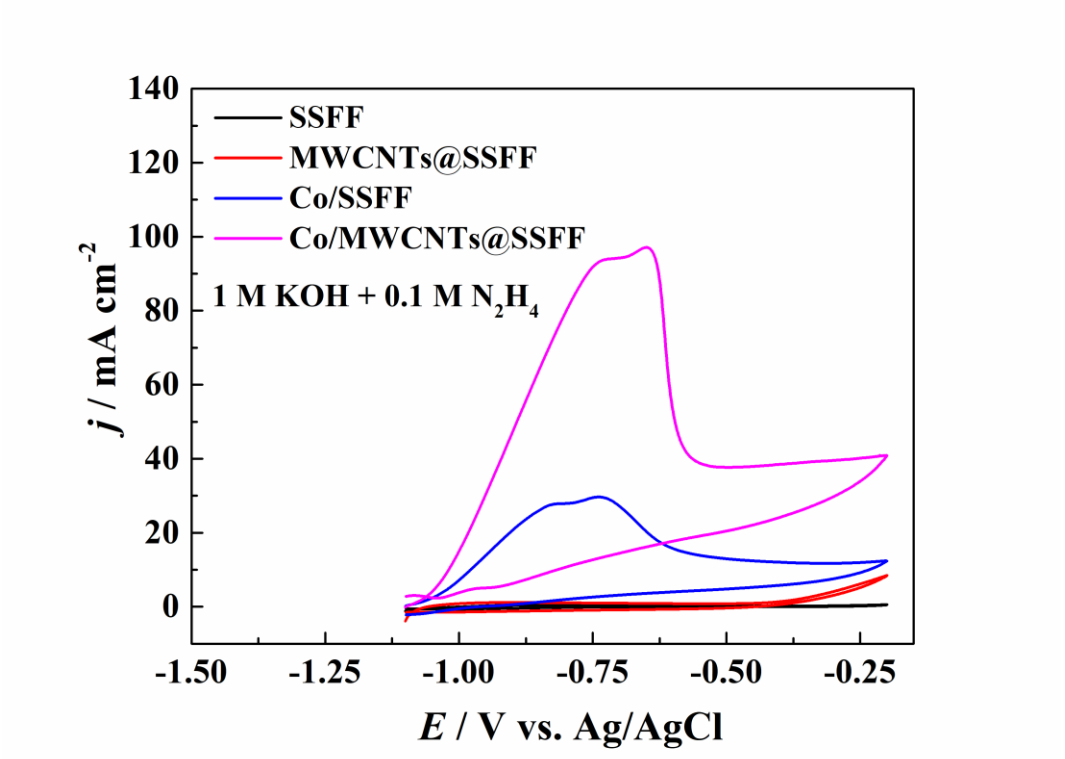

Figure 5. Cyclic voltammograms of the SSFF, MWCNTs@SSFF, Co/SSFF and Co/MWCNTs@SSFF electrodes in 1 M KOH with 0.1 M N_2H_4 at 10 mV s^{-1}.

Table 1. Comparison of the electrocatalytic performance of the Co/MWCNTs@SSFF electrode with that of some cobalt-based catalysts and metal nanoparticles supported on MWCNTs catalysts reported in the literature for N_2H_4 electrooxidation.

Catalysts	Electrolyte	[N_2H_4] (M)	Scan rate (mV s^{-1})	E_p (V vs. Ag/AgCl)	j_p (mA cm^{-2})	References
Ni_8Co_2/FMNSC	1 M KOH	0.1	20	Not provided	23.16	[8]
G(CN)-Co	PBS(pH 7.4)	0.05	10	-0.1[a]	3.5	[9]
Co/CFC	1 M KOH	0.02	10	-0.75	22	[29]
Ni_1Co_3 pompoms	1 M KOH	0.1	20	Not provided	42.7	[30]
Pd-Co/MWCNTs	1 M NaOH	0.02	10	-0.72	51[b]	[31]
Ni-MWNTs-textile	1 M NaOH	0.02	10	-0.76	12	[32]
Co/MWCNTs@SSFF	1 M KOH	0.1	10	-0.65	97.1	This work

E_p: peak potential for N_2H_4 oxidation; j_p: peak current density for N_2H_4 oxidation.

[a] The reported potential was relative to SCE.

[b] j_p was expressed as mA mg^{-1}.

The ECSA can be viewed as an important factor that affects the electrocatalytic activity of an electrode. The ECSA of the Co/MWCNTs@SSFF and Co/SSFF samples can be evaluated through their double layer capacitance (C_{dl}). To thoroughly understand the superior electrocatalytic activity of Co/MWCNTs@SSFF, cyclic voltammograms of the Co/SSFF (Fig. 6a) and Co/MWCNTs@SSFF (Fig. 6b) samples in the range of -0.25 ~ -0.15 V at various scanning speeds in 1 M KOH were measured. Based on the formula (Eq. (4)) [33], the C_{dl} value was obtained from the corresponding plot of the current density ($\triangle j$) at -0.2 V against the scanning speed (v) (Fig. 6c). The C_{dl} values of the Co/SSFF and Co/MWCNTs@SSFF samples are 0.0016 and 0.0155 F cm^{-2}, respectively. Because the ECSA is directly proportional to the C_{dl} [11,34], the ECSA of the Co/MWCNTs@SSFF sample is 9.7 times larger than that of the Co/SSFF sample, which demonstrates that the introduction of MWCNTs can remarkably boost the surface area. The Co/MWCNTs@SSFF sample, with its large ESCA, can provide more active sites for catalyzing N_2H_4 oxidation, thus significantly improving the catalytic performance of the electrode.

$$dj = C_{dl}dv \quad (4)$$

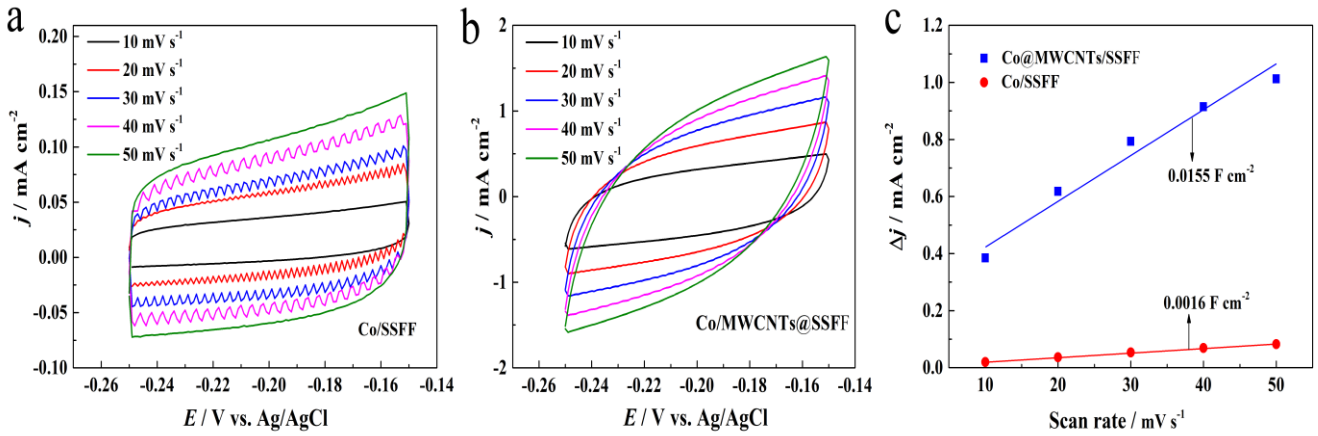

Figure 6. Cyclic voltammograms of the Co/SSFF (a) and Co/MWCNTs@SSFF (b) samples in the range of -0.25 ~ -0.15 V at various scanning speeds in 1 M KOH. Plot of current density ($\triangle j$) at -0.2 V against scanning speed (c).

The electrocatalytic stability of the Co/MWCNTs@SSFF sample was researched using a chronoamperometric curve. Figure 7 displays the chronoamperometric curve obtained with the Co/MWCNTs@SSFF sample at -0.7 V in 1 M KOH and 0.1 M N_2H_4. The current density decreases quickly in the initial few minutes, then little change occurs during the remaining test time. The result demonstrates that the electrocatalytic stability of the as-synthesized Co/MWCNTs@SSFF sample is good.

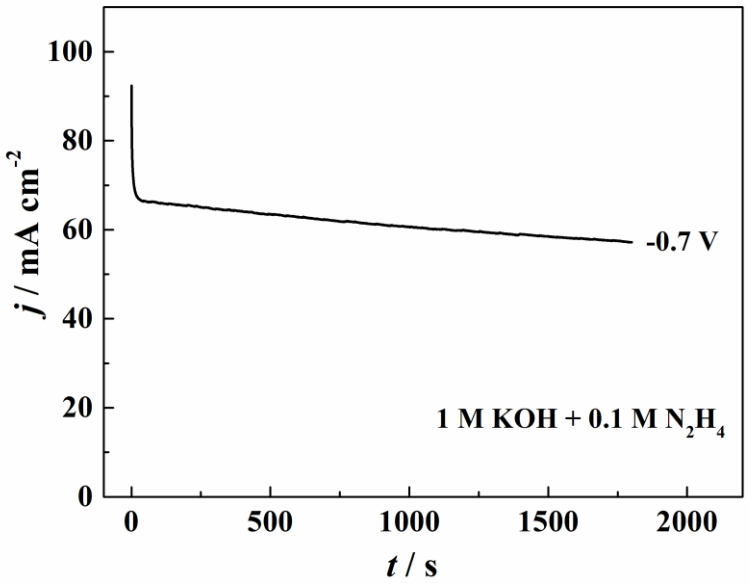

Figure 7. Chronoamperometric curve of the Co/MWCNTs@SSFF sample in 1 M KOH with 0.1 M N_2H_4 at -0.7 V.

The electrocatalytic property of the Co/MWCNTs@SSFF sample was further studied. A series of cyclic voltammograms of the as-obtained Co/MWCNTs@SSFF sample in 1 M KOH along with various N_2H_4 concentrations (0.01, 0.02, 0.03, 0.04 M) at 10 mV s^{-1} were obtained (Fig. 8a). Along with the augment in N_2H_4 concentration, the N_2H_4 oxidation peak current density presents a gradually increasing trend, and the peak potential shows a trend of a continuously positive shift. This result reveals that the N_2H_4 electrooxidation process on the Co/MWCNTs@SSFF sample is subject to mass transfer control.

A graph (Fig. 8b) was drawn with the logarithm of N_2H_4 concentration (log$C$(N_2H_4)) as the X-axis and the logarithm of current densities at -0.75 V (log$j$) as the Y-axis. The graph displays a good linearity between log$j$ and log$C$(N_2H_4). The line has a slope of 0.9. In accordance with the formula (Eq. (5)), the reaction order n is approximately equal to 1, which shows that the N_2H_4 electrooxidation process on the Co/MWCNTs@SSFF sample follows first-order kinetics with reference to N_2H_4.

$$n_i = \left(\frac{\partial \log j}{\partial \log C_i} \right)_{E,C_j} \quad (5)$$

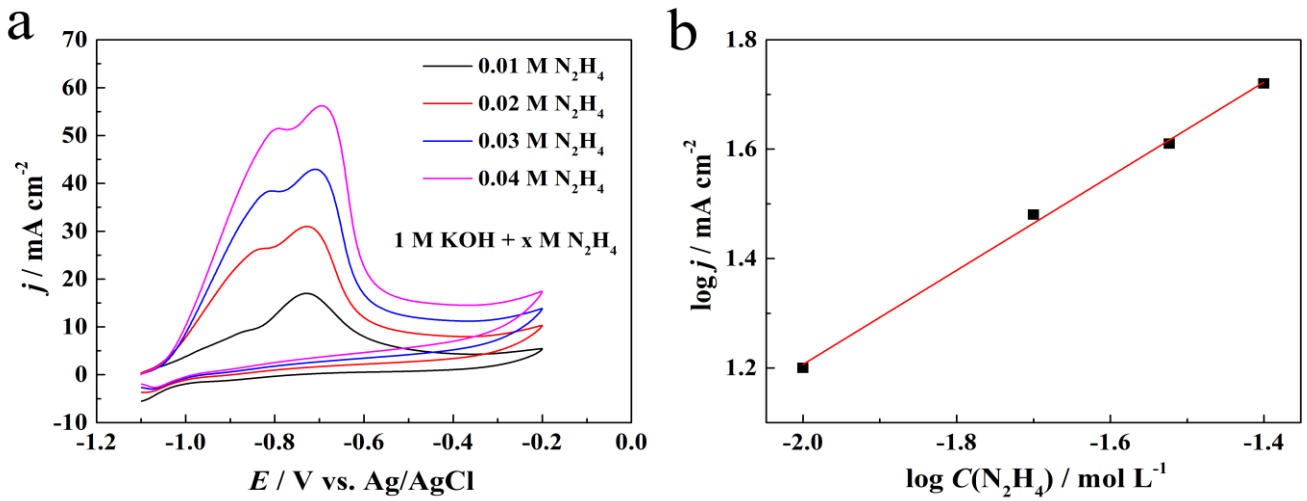

Figure 8. Series of cyclic voltammograms of the Co/MWCNTs@SSFF sample in 1 M KOH along with various N_2H_4 concentrations (0.01, 0.02, 0.03, 0.04 M) at 10 mV s^{-1}(a). Plot of log$j$ at -0.75 V versus log$C$(N_2H_4) (b).

A series of cyclic voltammograms of the Co/SSFF (Fig. 9a) and Co/MWCNTs@SSFF electrodes (Fig. 9b) in 1 M KOH and 0.1 M N_2H_4 at a scanning speed of 10 mV s^{-1}, and various temperatures were obtained. As the temperature is increased, the peak current densities of N_2H_4 oxidation and H_2 oxidation on the Co/MWCNTs@SSFF and Co/SSFF samples both display a tendency of gradually increasing, indicating that elevating the temperature is beneficial to increasing the rates of the N_2H_4 electrooxidation reaction and N_2H_4 decomposition reaction. The E_a values of the N_2H_4 electrochemical oxidation reaction on the Co/MWCNTs@SSFF and Co/SSFF samples were obtained with the Arrhenius formula (Eq. (6)).

$$\ln j = -E_a / RT + \ln A \quad (6)$$

A plot of the logarithm of N_2H_4 oxidation current densities (ln$j$) at -0.65 V (N_2H_4 oxidation peak potential at 296 K) on the Co/MWCNTs@SSFF sample against the reciprocal of the absolute temperature ($1/T$) is given in Fig. 9c. For comparison, the plot of ln$j$ at -0.7 V (N_2H_4 oxidation peak potential at 296 K) on the Co/SSFF sample against $1/T$ is also provided in Fig. 9c. Linear fitting was carried out to obtain the line slope. The E_a of the N_2H_4 electrooxidation reaction on the as-synthesized Co/MWCNTs@SSFF sample was 16.2 kJ mol^{-1}. The E_a of Co/MWCNTs@SSFF is far below that of the Co/SSFF sample (26.3 kJ mol^{-1}). This result suggests that the N_2H_4 electrooxidation kinetics on the Co/MWCNTs@SSFF sample is faster in comparison with the Co/SSFF sample.

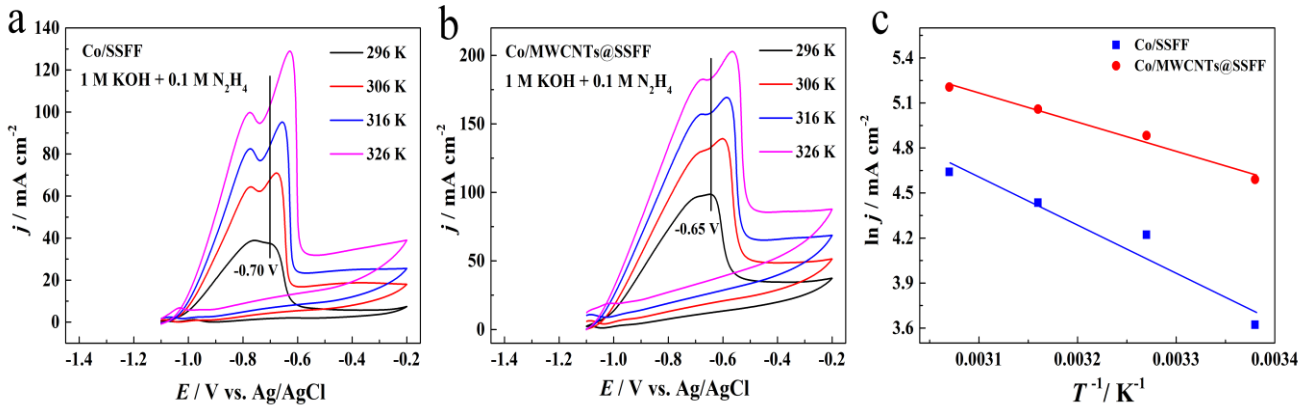

Figure 9. Cyclic voltammograms obtained on the Co/SSFF (a) and Co/MWCNTs@SSFF (b) electrodes in 1 M KOH with 0.1 M N_2H_4 at various temperatures (296 K, 306 K, 316 K, 326 K) at 10 mV s^{-1}. Arrhenius plots for the Co/MWCNTs@SSFF sample at -0.65 V and the Co/SSFF sample at -0.7 V (c).

4. CONCLUSIONS

In this study, by dipping a bare SSFF substrate into a MWCNT suspension followed by the electrodeposition of Co, Co nanospheres were successfully grown on the MWCNT-coated fibers of the SSFF. Compared to the Co/SSFF sample, the Co/MWCNTs@SSFF sample exhibited a better electrocatalytic performance toward N_2H_4 electrooxidation. Additionally, the E_a of the Co/MWCNTs@SSFF sample was smaller than that of the Co/SSFF sample. The superior electrocatalytic property of the as-obtained Co/MWCNTs@SSFF sample could be largely attributed to the macroporous structure of the SSFF substrate, the porous structure of the Co nanospheres, and the increased ECSA derived from the MWCNT modification. The porous structure of the Co/MWCNTs@SSFF sample not only made N_2H_4 more easily accessible to the surface and accelerated the electrode/electrolyte interfacial reaction rate but also ensured that the gas products quickly left the electrode surface.

ACKNOWLEDGMENTS
This work was supported by the Innovation and Entrepreneurship Training Program for College Students in Heilongjiang Province (202010234044).

References

1. K. Yamada, K. Asazawa, K. Yasuda, T. Ioroi, H. Tanaka, Y. Miyazaki and T. Kobayashi, *J. Power Sources*, 115 (2003) 236.
2. K. Yamada, K. Yasuda, H. Tanaka, Y. Miyazaki and T. Kobayashi, *J. Power Sources*, 122 (2003) 132.
3. S. M. Ji, Z. K. Ghouri, K. Elsaid, Y. H. Ko, S. Al-Meer, M. I. Ahmad, D. I. Son and H. Y. Kim, *Int. J. Electrochem. Sci.*, 12 (2017) 2583.
4. V. Rosca and M. T. M. Koper, *Electrochim. Acta,* 53 (2008) 5199.
5. M. G. Hosseini, S. Zeynali, M. M. Momeni, and R. Najjar, *J. Appl. Polym. Sci.*, 124 (2012) 4671.
6. F. Liu, X. Jiang, H. H. Wang, C. Chen, Y. H. Yang, T. Sheng, Y. S. Wei, X. S. Zhao and L. Wei, *ACS Sustain. Chem. Eng*., 10 (2022) 696.
7. H. Wang, J. T. Ding, P. Kannan and S. Ji, *Int. J. Hydrogen Energy*, 45 (2020) 19344.
8. J. Y. Zhang, J. S Li and C. D Huang, *Int. J. Electrochem. Sci.*, 13 (2018) 1787.
9. R. G. Kadam, T. Zhang, D. Zaoralova, M. Medved, A. Bakandritsos, O. Tomanec, M. Petr, J. Z. Chen, J. T. Miller, M. Otyepka, R. Zboril, T. Asefa and M. B. Gawande, *Small*, 17 (2021) 2006477.
10. S. Chen, C. L. Wang, S. Liu, M. X. Huang, J. Lu, P. P. Xu, H. G. Tong, L. Hu and Q. W. Chen, *J. Phys. Chem. Lett*., 12 (2021) 4849.
11. H.H. Jiang, Z.N. Wang, P. Kannan, H. Wang, R.F. Wang, P. Subramanian and S. Ji, *Int. J. Hydrogen Energy*, 44 (2019) 24591.
12. G. Feng, Y. Kuang, Y. J. Li and X. M. Sun, *Nano Res.*, 8 (2015) 3365.
13. J. Zhang, X. Y. Cao, M. Guo, H. N. Wang, M. Saunders, Y. Xiang, S. P. Jiang and S. F. Lu, *ACS Appl. Mater. Inter.*, 11 (2019) 19048.
14. T. Y. Jeon, M. Watanabe and K. Miyatake, *ACS Appl. Mater. Inter.*, 6 (2014) 18445.
15. H. Wen, L. Y. Gan, H. B. Dai, X. P. Wen, L. S. Wu, H. Wu and P. Wang, *Appl. Catal. B-Environ.*, 241 (2019) 292.
16. T. Sakamoto, K. Asazawa, J. Sanabria-Chinchilla, U. Martinez, B. Halevi, P. Atanassov, P. Strasser and H. Tanaka, *J. Power Sources*, 247 (2014) 605.
17. T. Sakamoto, D. Matsumura, K. Asazawa, U. Martinez, A. Serov, K. Artyushkova, P. Atanassov, K. Tamura, Y. Nishihata and H. Tanaka, *Electrochim. Acta*, 163 (2015) 116.
18. X. L. Wang, Y. X. Zheng, M. L. Jia, L. S. Yuan, C. Peng and W. H. Yang, *Int. J. Hydrogen Energy*, 41 (2016) 8449.
19. Z. B. Feng, D. G. Li, L. Wang, Q. Sun, P. Lu, P. F. Xing and M. Z. An, *Electrochim. Acta*, 304 (2019) 275.
20. X. H. Gao, C. Du, C. M. Zhang and W. Chen, *ChemElectroChem*, 3 (2016) 1266.
21. B. Filanovsky, E. Granot, I. Presman, I. Kuras and F. Patolsky, *J. Power Sources*, 246 (2014) 423.
22. K. Asazawa, T. Sakamoto, S. Yamaguchi, K. Yamada, H. Fujikawa, H. Tanaka and K. Oguro, *J. Electrochem. Soc.*, 156 (2009) B509.
23. K. Asazawa, K. Yamada, H. Tanaka, M. Taniguchi and K. Oguro, *J. Power Sources*, 191 (2009) 362.
24. W. W. Chen, Z. L. Liu, Y. X. Li, K. J. Jiang, J. X. Hou, X. G. Lou, X. Y. Xing, Q. Liao and X. Zhu, *Electrochim. Acta*, 324 (2019) 134862.
25. J. X. Hou, Z. L. Liu, S. Q. Yang and Y. Zhou, *J. Power Sources*, 258 (2014) 204.
26. D. M. Zhang, K. Cheng, N. N. Shi, F. Guo, G. L. Wang and D. X. Cao, *Electrochem. Commun*., 35 (2013) 128.
27. S. L. Zhu, C. P. Chang, Y. Z. Sun, G. Y. Duan, Y. M. Chen, J. Q. Pan, Y. Tang and P. Y. Wan, *Int. J. Hydrogen Energy*, 45 (2020) 1810.
28. F. Yang, B. Cao, Y. Tao, M. Hu, C. C. Feng, L. Wang, Z. Jiang, D. X. Cao and Y. Zhang. *J. Power Sources*, 298 (2015) 38.
29. R. Liu, X. Jiang, F. Guo, N. N. Shi, J. L. Yin, G. L. Wang and D. X. Cao, *Electrochim. Acta*, 94 (2013) 214.

30. H. Wang, Y. J. Ma, R. F. Wang, J. L. Key, V. Linkov and S. Ji, *Chem. Commun.*, 51 (2015) 3570.
31. J. Liu, R. Liu, C. L. Yuan, X. P. Wei, J. L. Yin, G. L. Wang and D. X. Cao, *Fuel Cells*, 13 (2013) 903.
32. D. D. Zhang, B. Wang, D. X. Cao, K. Ye, Y. Xu, J. L. Yin, K. Cheng and G. L. Wang, *Mater. Sci. Eng. B-Adv.*, 188 (2014) 48.
33. B. P. Li, C. Y. Song, J. L. Yin, J. Yan, K. Ye, K. Cheng, K. Zhu, D. X. Cao and G. L. Wang, *Int. J. Hydrogen Energy*, 45 (2020) 10569.
34. Y. C. Xie, Z. N, Wang, H. Wang, L. Lu, P. Subramanian, S. Ji and P. Kannan, *ChemElectroChem*, 8 (2021) 937.